

## Electron transport and superconductivity in amorphous Sb and its alloys

J. J. Hauser

Bell Laboratories, Murray Hill, New Jersey 07974

(Received 9 July 1974)

Amorphous Sb and its alloys are shown to be similar to amorphous Ge from studies of resistivity and electron tunneling. The localization behavior for impurity states in amorphous Sb follows the same general rules as observed for the localization of impurity states in amorphous Ge. Even though crystalline Sb is a semimetal, amorphous Sb is found to be a semiconductor with properties similar to the amorphous tetrahedrally bonded semiconductors.

### I. INTRODUCTION

It has been recently shown<sup>1</sup> that conductivity in amorphous antimony takes place via a thermally activated hopping mechanism between localized states<sup>2</sup> similar to the one described in amorphous tetrahedrally bonded semiconductors.<sup>3-5</sup> Indeed, the low-temperature resistivity of all amorphous Sb films regardless of the method of deposition (getter sputtering, evaporation from Sb, and evaporation from PtSb) was fitted<sup>1</sup> quite accurately by the relation

$$\rho = \rho_0 e^{(T_0/T)^{1/4}}, \quad (1)$$

where  $T_0$ , given by the expression

$$T_0 = 16\alpha^3 / N(E_F)k, \quad (2)$$

was approximately  $10^7$  °K. In relation (2)  $\alpha$  is the coefficient of exponential decay of localized-state wave functions,  $N(E_F)$  is the density of localized states at the Fermi level, and  $k$  is Boltzmann's constant. If one uses  $\alpha = 10^7$  cm<sup>-1</sup>, the experimental value  $T_0 = 10^7$  °K corresponds via relation (2) to approximately  $10^{19}$  states/eV cm<sup>3</sup>. This is about the same order of magnitude as that reported for amorphous tetrahedrally bonded semiconductors.<sup>3-5</sup>

From the structural point of view, a broken-layer structure has been suggested for amorphous antimony ( $\alpha$ -Sb) by x-ray diffraction studies.<sup>6</sup> Crystalline Sb consists of weakly bonded double layers with threefold-coordinated Sb. Richter *et al.*<sup>6</sup> observed that the first- and third-coordination spheres which pertain to atoms within the double layers are retained in  $\alpha$ -Sb. The second coordination is changed, showing the randomness of the relative positions of neighboring double layers. However, a more recent study by Krebs and Steffen<sup>7</sup> concludes that one can only ascertain from the atomic distribution curve the threefold coordination of Sb and the presence of more distant neighbors which are about 3.64 Å apart and more weakly bound. At any rate, it is clear from both studies<sup>6,7</sup> that, similar to the case of amorphous tetrahedrally bonded semiconductors (Ge and Si), the first-coordination sphere is

conserved in  $\alpha$ -Sb. Such a structural model is satisfactory for  $\alpha$ -Ge and  $\alpha$ -Si where the amorphous state can be described<sup>8</sup> as a semiconductor with a pseudogap comparable in magnitude to the gap present in the crystalline state. In other words, for both structural and electrical properties,  $\alpha$ -Ge and  $\alpha$ -Si can be considered as perturbations of the crystalline state. On the other hand, the situation is very different for Sb, which in the crystalline state is a semimetal with a small band overlap<sup>9</sup> (about 25 meV), while the electrical properties<sup>1</sup> suggest that the  $\alpha$ -Sb can be characterized as a semiconductor with a large pseudogap comparable to that of  $\alpha$ -Ge. This would in turn suggest that the atomic arrangement in the amorphous state should be appreciably different from that of the crystalline state. It could also suggest that the electronic configurations differ, i. e., lone-pair  $p$  states in Sb and  $sp^3$  directed bonds in  $\alpha$ -Ge and  $\alpha$ -Si.

In order to study further the similarities between  $\alpha$ -Sb and  $\alpha$ -Ge, the present study will be concerned with tunneling studies and alloying experiments similar to those already reported for  $\alpha$ -Ge.<sup>10,11</sup>

### II. EXPERIMENTAL PROCEDURE

All Sb-alloy films were deposited at 77 °K by getter sputtering from arc-melted alloys which were subsequently inductively melted in a graphite crucible.<sup>12</sup> While Sb-rich alloys were always sputtered at 2 W (1000 V, 2 mA) in a pure argon atmosphere at a pressure of  $1.5 \times 10^{-2}$  Torr, Bi films and Bi-rich-alloy films were also sputtered in argon-hydrogen mixtures at the same total pressure ( $1.5 \times 10^{-2}$  Torr) and at the same power of 2 W. The hydrogen partial pressure was approximately 3%. Although there is some scatter in the deposition rates of the films, hydrogen has a marked effect on the deposition rate, namely, the rate is 280 Å/min for Bi films sputtered in pure argon and 240 Å/min for films sputtered in a 3% hydrogen-argon mixture. Sb-Ni alloy films were prepared in two different ways: first, from alloy targets as mentioned above, and second, from composite targets where 0.028-in. -

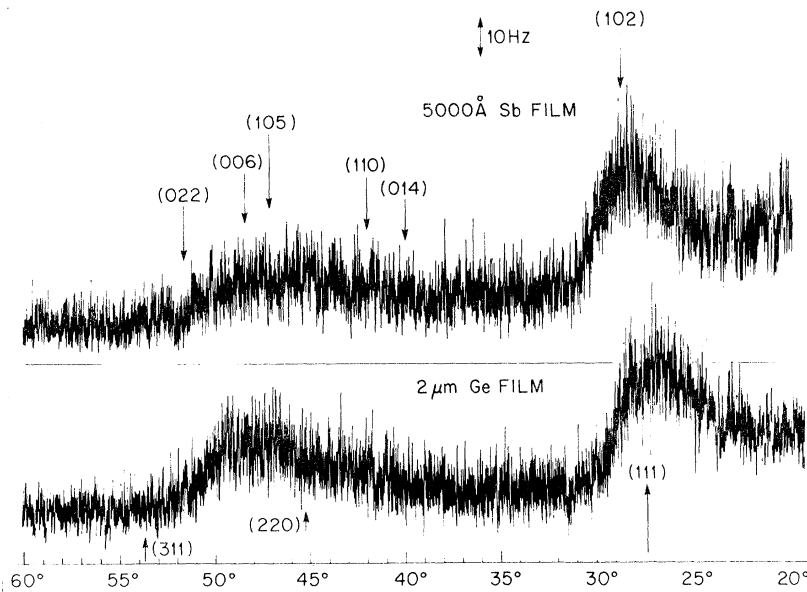


FIG. 1. X-ray diffractometer traces taken at 300°K for two films deposited at 77°K; the top trace pertains to an Sb film, the bottom one to a Ge film. The crystalline lines are indicated by arrows.

diam Ni rods were uniformly embedded in a 2.25-at.-%-Ni-alloy target. This composite-target technique has been shown to give films with uniform composition in the case of dilute alloys.<sup>11,13</sup> The composition of all targets and of certain films was checked by x-ray fluorescence analysis. The amorphous structure of the films was established by x-ray diffractions. The thickness of all films was approximately 3000 Å. The Sb tunnel junctions were prepared identically to the previously described *a*-Ge junctions.<sup>11</sup> All the films were transferred under liquid nitrogen onto the resistivity holder, which was then immersed in liquid helium. The resistivity of the film was then measured in helium gas by warming up to room temperature.

### III. EXPERIMENTAL RESULTS AND DISCUSSION

#### A. X-ray diffraction

The x-ray diffraction trace taken at room temperature on a 5000-Å Sb film deposited at 77°K is shown in Fig. 1. The x-ray diffractions obtained on all Sb-rich-alloy films are quite similar to the pattern shown in Fig. 1, which is characteristic of an amorphous film. The diffraction pattern for *a*-Sb, which is in good agreement with previous studies,<sup>6,7</sup> is compared in Fig. 1 with the pattern for *a*-Ge. It is clear from Fig. 1 that in both cases (*a*-Sb and *a*-Ge) the first broad diffraction peak occurs very close to the respective strongest crystalline diffraction line. The next broad peak in *a*-Ge is positioned between the next two strongest crystalline lines. On the other hand, the second broad diffraction peak of *a*-Sb does not occur next to the second strongest crystalline lines [(014) and (110)],<sup>14</sup> but instead falls at an angular value close

to that of the second broad peak of *a*-Ge. Richter *et al.*,<sup>6</sup> using Fourier-transform analysis on data similar to those shown in Fig. 1, concluded that the nearest-neighbor distance is the same in amorphous and crystalline Sb, while the second-coordination sphere which pertains to Sb atoms in neighboring double layers is changed in the amorphous state. At any rate, the patterns for *a*-Sb and *a*-Ge are very similar and certainly the pattern for *a*-Sb bears a closer resemblance to that of *a*-Ge than to that of crystalline Sb. This is not meant to suggest that Sb atoms are fourfold coordinated in the amorphous state, as previous studies<sup>6,7</sup> suggested that Sb remains threefold coordinated in the amorphous state. The similarity of the patterns shown in Fig. 1 might suggest that, in analogy with *a*-Ge, *a*-Sb can be described by a random network of threefold-coordinated atoms. One may speculate that a random network is more important than the exact structure or coordination in determining the electrical properties of the amorphous state. That is, the similarity between the diffraction patterns of *a*-Sb and *a*-Ge may be the underlying reason for the similarity in their electrical properties (Ref. 1 and Secs. III C and IIID of the present paper).

#### B. Ga-Sb and Bi-Sb alloys

Ferrier and Herrell reported the conductivity of amorphous Mg-Sb alloys.<sup>15</sup> The Mg-rich alloys are metallic up to 40 at.-% Sb (corresponding to Mg<sub>3</sub>Sb<sub>2</sub>), while alloys with higher Sb concentrations are semiconducting with an activation energy of 0.5–0.2 eV. We would suggest that such behavior is quite general for amorphous Sb alloys, but that

the concentration at which an energy gap develops depends on the chemical bonding between Sb and the other atom. It is necessary for such a study to use alloys that can be made amorphous over the entire composition range. This is why Ga and Bi were chosen. Amorphous Ga and Bi films are superconducting<sup>16</sup> with respective transition temperatures ( $T_c$ ) of 8, 4 and 6 °K, while crystalline Ga has a  $T_c$  of 1.07 °K and crystalline Bi is not superconducting at all. Amorphous superconducting films are usually obtained by evaporation onto substrates held at liquid-helium temperatures.<sup>16</sup> In the case of Ga, amorphous films with a  $T_c$  of 7.2 °K have been obtained by evaporation in a partial oxygen pressure<sup>17</sup> on substrates held at room temperature. In the present study the Ga and Ga-Sb films were sputtered at 77 °K, which resulted in  $T_c$ 's as high as 8 °K for pure amorphous Ga films. The transition temperature for amorphous Ga-Sb films is shown as a function of Sb concentration in Fig. 2. Also shown is the resistivity of these films, which increases rapidly with increasing Sb content and increases discontinuously by several orders of magnitude at the GaSb composition. The films are metallic (positive temperature coefficient of resistance) up to 30 at.% Sb; above 30 at.% up to 50 at.% Sb the films display a small negative temperature coefficient of resistance still consistent with zero energy gap. All these observations can be understood in terms of an increasing number of Ga-Sb bonds with increasing Sb content until the disappearance of superconductivity in the vicinity of the GaSb composition. The electrical properties

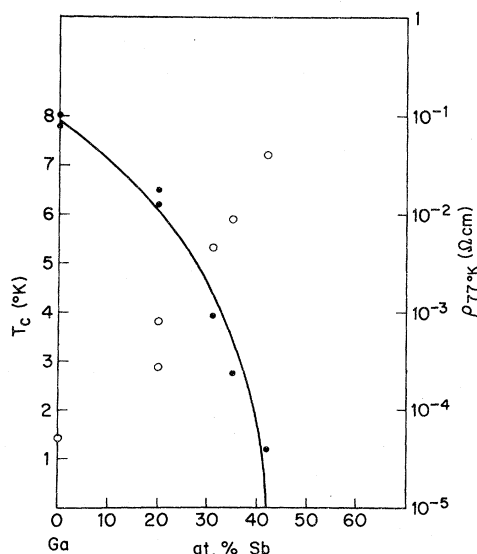


FIG. 2. Transition temperature and resistivity of Ga-Sb alloys as a function of Sb concentration. Solid circles,  $T_c$ ; open circles,  $\rho$ .

of Ga-Sb films on the Sb-rich side of GaSb are very similar to those of InSb films.<sup>18</sup> As-deposited  $\text{Ga}_{0.4}\text{Sb}_{0.6}$  films are characterized by a hopping conductivity via localized states; the resistivity can be fitted by relation (1) with  $T_0 = 2.4 \times 10^8$  °K, which corresponds via relation (2) to about  $10^{18}$  states/eV  $\text{cm}^3$ . After annealing to room temperature, the resistivity depends exponentially on temperature with an energy gap of 0.52 eV. Therefore, just as in the Mg-Sb system, the change from metallic to semiconducting behavior occurs at the intermetallic composition. In order to isolate the effect of the statistical environment of an Sb atom, one should investigate an Sb alloy where there is no intermetallic compound. This is the case for Bi-Sb alloys which form a complete series of solid solutions.

Amorphous Bi films with a  $T_c$  of 6 °K obtained by evaporation at 4 °K revert to the nonsuperconducting crystalline form of Bi when heated above 15 °K.<sup>16</sup> Coevaporation<sup>19</sup> at 4 °K of mixtures of Bi with either Cu, LiF, or Sb leads to a decrease of  $T_c$  with a concomitant increase in the recrystallization temperature. The superconducting amorphous Bi films of the present study were obtained by a new method consisting of getter sputtering Bi at 77 °K in an argon-hydrogen mixture. The presence and concentration of hydrogen is critical in obtaining amorphous superconducting Bi films. The optimum concentration seems to consist of 3% partial pressure of hydrogen in argon. A higher partial pressure of hydrogen (by only a few percent) results in no film deposit at all. A lower partial pressure of hydrogen (e.g., 2% and below) results in crystalline nonsuperconducting films with a resistivity approximately six times higher than that of the amorphous superconducting ones (see Fig. 3 at 0 at.% Sb). Although there is no explanation for the crucial effect of hydrogen, the small amount of hydrogen must produce the amorphous state of the films by altering film growth, as evidenced by the definitely lower deposition rate (15%) for a 3% hydrogen-argon mixture as compared to pure argon. The rate itself is not the explanation, since sputtering Bi at even half the rate (by using half the power) still results in nonsuperconducting crystalline Bi films. One should stress that the critical hydrogen partial pressure (3%) discussed above is only pertinent for a 2-W sputtering power and a total pressure of  $1.5 \times 10^{-2}$  Torr. It is also interesting to point out that the recrystallization temperature for the amorphous films is appreciably higher than previously reported<sup>16,19</sup> (about 200 °K); above 200 °K the resistance of the films increases in an irreversible manner and the films revert to the normal crystalline nonsuperconducting form of Bi. The highest transition temperature attained for these amorphous Bi films was 5.65 °K.

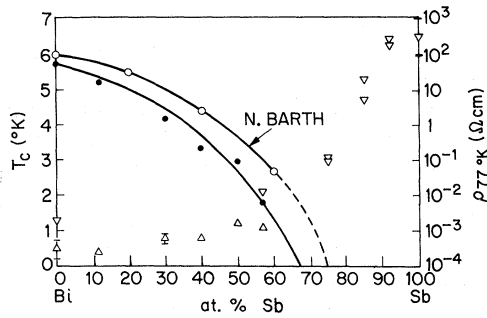


FIG. 3. Transition temperature and resistivity of Bi-Sb alloys as a function of Sb concentration. Solid circles,  $T_c$ , this study; open circles,  $T_c$  of Ref. 19; up triangles,  $\rho$  for superconducting films; down triangles,  $\rho$  for non-superconducting films.

The dependence of  $T_c$  on Sb concentration for Bi-Sb amorphous films sputtered at 77° K in an argon-hydrogen atmosphere is shown in Fig. 3. These results are in good agreement with Barth's films,<sup>19</sup> which were evaporated at 4° K. Superconductivity disappears at about 67 at. % Sb. The resistivity at 77° K for amorphous Bi-Sb films increases with Sb concentration (Fig. 3) and reaches the resistivity of a nonsuperconducting Bi film (deposited in pure argon) at about the concentration where superconductivity disappears (67 at. %). Above 67 at. % Sb the Bi-Sb films are no longer superconducting and their resistivity increases rapidly with Sb concentration. It is interesting to note that the curve (not drawn in Fig. 3) which best averages the resistivity of Sb-rich films intersects the resistivity of superconducting films ( $\approx 10^{-3} \Omega \text{ cm}$ ) in the vicinity of the critical concentration (67 at. %). Bi-Sb films with more than 67 at. % Sb are characterized by a thermally activated hopping conductivity via localized states. Their low-temperature resistivity is well fitted by relation (1) and  $T_0$  increases rapidly from  $10^4$  to  $10^7$ ° K (the value for pure  $\alpha$ -Sb) as Sb increases from 75 to 92 at. %. The increase in  $T_0$  or decrease in  $N(E_F)$  with decreasing Bi content does not imply that Bi acts as a localized impurity state in Sb. Indeed, as shown in Fig. 4,  $T_0$  has the same value for  $\text{Sb}_{0.92}\text{Bi}_{0.08}$  as for pure  $\alpha$ -Sb, while 8 at. % Bi is more than sufficient to reveal localization if present (see Sec. III C and Refs. 10 and 11). The increase in  $T_0$  with increasing Sb above 67 at. % Sb would be consistent with the progressive opening up of the pseudogap, although other explanations are equally possible. The Bi-Sb alloy experiments which are not obscured by the formation of any intermetallic compound can be simply explained in terms of the concentration of Sb-Sb pairs. Starting from pure Bi, increasing the Sb concentration increases the number of Sb-Sb pairs, thereby de-

creasing  $T_c$  and slightly increasing  $\rho$ . This process goes on up to the critical concentration of 67 at. %, where superconductivity disappears; at this point the concentration of Sb-Sb pairs is sufficient to open up an energy gap between bonding and antibonding states. We shall now confine ourselves to  $\alpha$ -Sb alloys rich in Sb, which are therefore characterized by a pseudogap, in order to study which impurities lead to the formation of localized states near  $E_F$ .

### C. Localized and nonlocalized impurity states

A recent study<sup>10,11</sup> of impurities in  $\alpha$ -Ge showed that impurities can be divided in two classes. Impurities which produce deep energy levels in crystalline Ge form localized states near  $E_F$ , while impurities which produce shallow impurity levels in crystalline Ge do not. Impurities which do not form localized states are either isoelectronic with Ge (Si and Sn) or the typical acceptor (column-III) or donor (column-V) impurities. All impurities which form localized states near  $E_F$  behave in a similar manner.<sup>10,11</sup> There is no increase in the number of localized states  $[N(E_F)]$  up to about 6 at. % impurity; thereafter  $N(E_F)$  increases linearly with concentration, the slope of the line being consistent with one localized state per eV per impurity atom. The reason  $N(E_F)$  does not increase initially was speculatively attributed<sup>10</sup> to the fact that impurities go at first in a network of highly disordered material. We will now investigate the

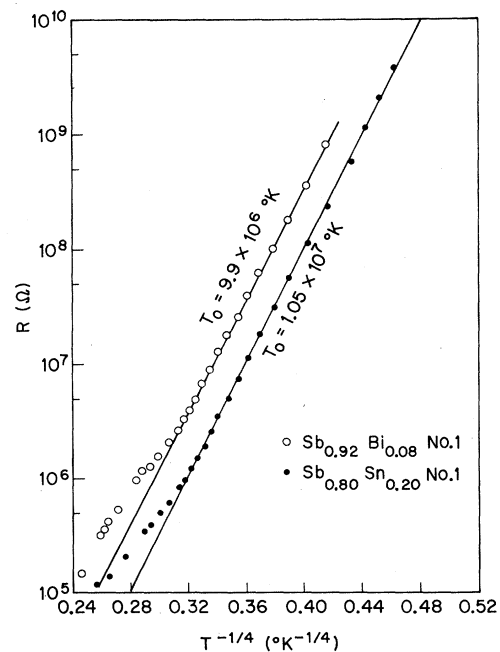


FIG. 4. Temperature dependence of the resistance for two  $\alpha$ -Sb alloys with  $T_0$  close to that of  $\alpha$ -Sb.

localization mechanism in *a*-Sb by first considering impurities which are likely not to form localized states.

It is already clear from the data shown in Fig. 4 that  $T_0$  remains unchanged by the addition of 8 at.% Bi. Actually, as shown in Table I, the density of localized states  $N(E_F)$  as obtained from  $T_0$  via relation (2) hardly increases with as much as 15 at.% Bi. The other isoelectronic element studied (As) behaves in a very similar fashion. Thus, as in *a*-Ge, isoelectronic impurities do not form localized impurity levels. In analogy with *a*-Ge one should now consider acceptor (column-IV) and donor (column-VI) impurities. The effect of Sn is shown in Fig. 4 where  $T_0$  has the same value as in pure *a*-Sb. The deviation towards higher resistance above 100 °K is caused by the same annealing effect observed<sup>1</sup> in *a*-Sb. The effect of Ge is studied as a function of Ge concentration in Fig. 5. It is clear from Fig. 5 that Ge does not form a localized impurity level at  $E_F$ . As a matter of fact,  $T_0$  increases with increasing Ge concentration, which, as shown in Table I, leads to the conclusion that the number of localized states decreases smoothly from the value<sup>1</sup> for pure *a*-Sb ( $10^{19}$ ) to the value<sup>4</sup> for pure *a*-Ge ( $10^{18}$ ). It is in-

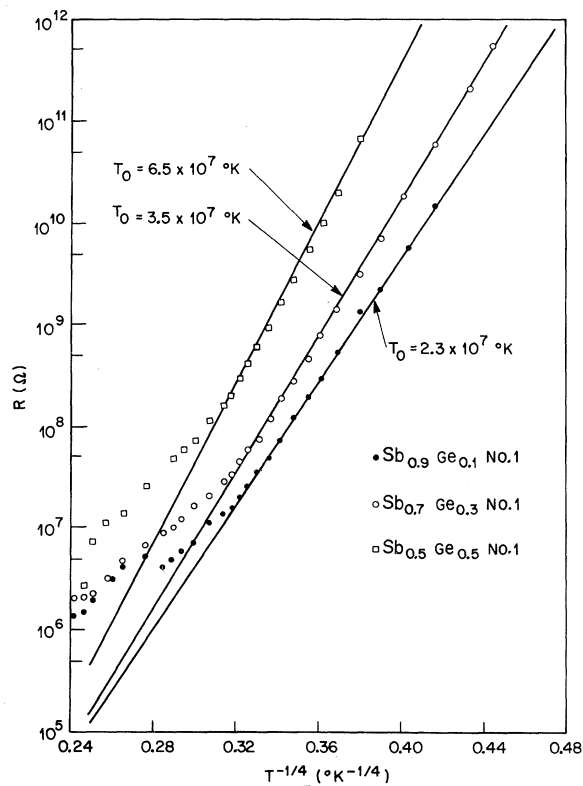


FIG. 5. Temperature dependence of the resistance for *a*-Sb-Ge alloys as a function of Ge concentration.

TABLE I.  $N(E_F)$  for Sb alloys with shallow-level impurities.

Impurity	Maximum concentration <sup>a</sup> (at. %)	Maximum $N(E_F)$ <sup>a</sup> ( $\text{eV cm}^{-3}$ ) <sup>-1</sup>
Ge	50 <sup>b</sup>	$2.9 \times 10^{18}$
Sn	20	$1.8 \times 10^{19}$
Bi	15	$6.6 \times 10^{19}$
As	20	$5.3 \times 10^{18}$

<sup>a</sup>This is the maximum concentration which displays the temperature-dependent resistivity of relation (1) and the corresponding  $N(E_F)$  obtained from relation (2).

<sup>b</sup> $N(E_F)$  decreases smoothly from the value for pure Sb ( $10^{19}$ ) to the value for pure Ge ( $10^{18}$ ) as the Ge concentration is increased from 0 to 100 at. %.

teresting to point out that, besides Ge-Si, Ge-Sb is another system where a complete series of amorphous semiconducting alloys can be obtained. In conclusion, isoelectronic and acceptor impurities do not form localized impurity states at  $E_F$  in *a*-Sb. It is more than likely that donor impurities<sup>20</sup> behave identically. In analogy with the *a*-Ge case, all these impurities (isoelectronic, acceptor, and donor) must form shallow impurity levels in the amorphous state.<sup>21</sup>

Impurities which are likely to form a localized impurity level at  $E_F$  should be chosen from such deep-energy-level impurities<sup>11</sup> as Ni. The temperature dependence of the resistance for *a*-Ge-Ni alloys is shown in Fig. 6. It is clear from Fig. 6 that  $T_0$  decreases monotonically with increasing Ni content; as we notice in Fig. 7, it is possible to observe nonmonotonic behaviors of  $T_0$  with concentration over small compositional variations of the order of 0.1 at. % simply as a result of not being able to ascertain the exact composition of all films to that accuracy. The density of localized impurity states at  $E_F$  is plotted as a function of Ni content in Fig. 7. While, as mentioned above, the films from alloy targets (solid dots) do not always yield a monotonic dependence of  $N(E_F)$  with Ni concentration, films from composite targets (open dots) behave monotonically even over small compositional variations of the order of 0.1 at. %. The composite targets were calibrated by setting the 2.25-at. %-Ni host target with 17 Ni rods equal to 3.1 at. %; this corresponds to each rod yielding 0.05 at. %, which is in good agreement with expectations from the ratio of sputtering areas and sputtering rates. The localization behavior of Ni in *a*-Sb and *a*-Ge is very similar. In both cases one does not obtain a localized state per eV per Ni atom (solid line in Fig. 7) from the onset. In other words, although Ni definitely gives rise to localized impurity levels, as shown by the increase in  $N(E_F)$  above 2.25 at. % Ni, there is hardly any increase

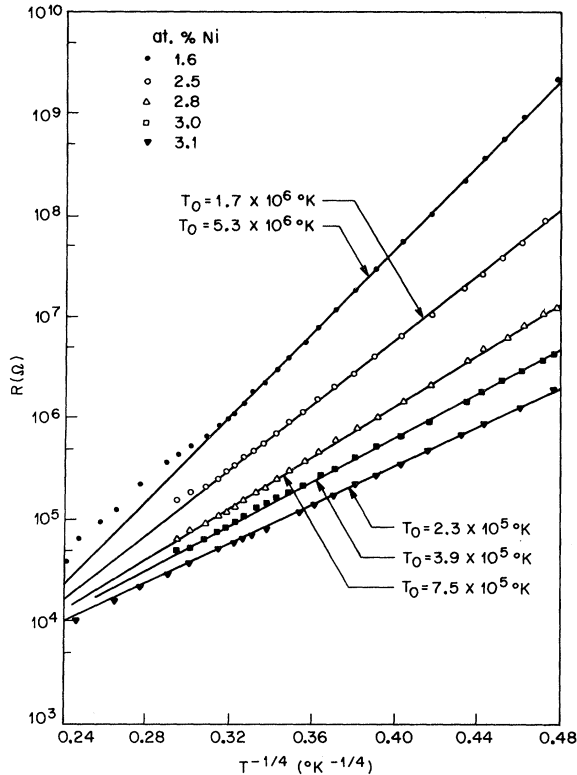


FIG. 6. Temperature dependence of the resistance for *a*-Sb-Ni alloys as a function of Ni concentration.

in  $N(E_F)$  for Ni concentrations below 2.25 at.%. Although there is not a definite explanation for this effect, one may speculate that, just as in the case of *a*-Ge,<sup>10</sup> the Ni impurities at first go into a network of highly disordered material. In *a*-Ge the network of highly disordered material was supposed to consist of the boundaries where the various growing amorphous islands impinge and which upon annealing at room temperature give rise to the network of voids.<sup>10</sup> One would expect that if such an explanation were correct, the onset of localization would be structure sensitive and therefore different for various *a*-semiconductors, as it is in the cases of *a*-Sb and *a*-Ge. At any rate, when the Ni concentration exceeds 2.25 at.% the data below the delocalization limit [especially the better data from the composite targets (open dots)] can be approximated by a straight line parallel to the solid line of Fig. 7 which corresponds to one localized state per eV per Ni atom. One may justifiably question the accuracy of this fit over such a small concentration range, but the fact that similar behavior was observed in *a*-Ge over a wider concentration range<sup>10,11</sup> further supports the above interpretation. The smaller range of concentrations available for localization studies in the

case of *a*-Sb results from the fact that, while the delocalization limit is approximately the same for *a*-Sb and *a*-Ge, the initial concentration of localized states is larger in *a*-Sb ( $10^{19}$ ) than in *a*-Ge ( $2 \times 10^{18}$ ). Indeed, the self-consistency of the theory<sup>22</sup> underlying relations (1) and (2) requires that, for impurities with a binding energy of 0.3 eV,  $T_0 > 7 \times 10^5$  °K or  $N(E_F) < 2.7 \times 10^{20}$  states/eV  $\text{cm}^3$ , at which point delocalization should occur. The faster rise in  $N(E_F)$  (or faster decrease in  $T_0$ ) above the delocalization limit (dashed line in Fig. 7) is the direct consequence of the decrease in  $\alpha$  which results from the progressive delocalization into extended states as the Ni concentration is increased. The *a*-Ge-Ni data were averaged by a straight line up to  $2 \times 10^{21}$  states (see Fig. 2 of Ref. 10) simply because of the greater scatter in the data. One could, however, analyze the *a*-Ge-Ni data in a manner very similar to that presented in Fig. 7 for *a*-Sb-Ni films. In summary, the localization of impurities in *a*-Sb follows the same general rules and concentration dependence as observed for impurities in *a*-Ge.<sup>10,11</sup>

#### D. Tunneling in *a*-Sb

The conductance versus bias obtained at 77 °K by hand differentiation of the *I*-*V* curve is shown in Fig. 8 for *a*-Ge and *a*-Sb tunnel junctions. As the tunneling-conductance-vs-voltage curves are nearly symmetric with respect to zero bias, we

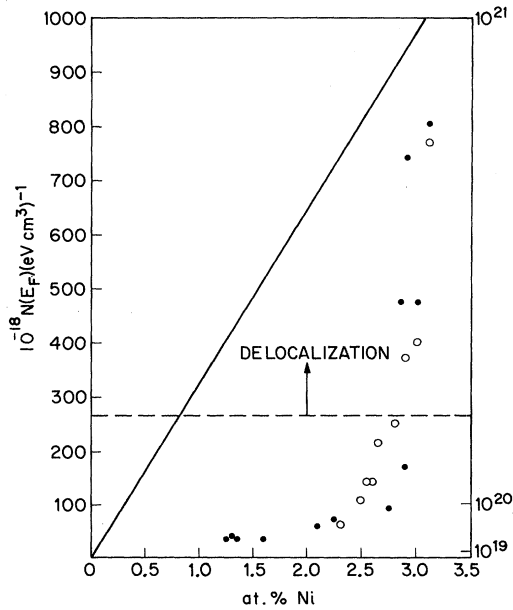


FIG. 7. Density of localized impurity states obtained from relation (2) with  $\alpha = 10^7 \text{ cm}^{-1}$  as a function of Ni concentration. The solid line corresponds to one localized state per eV per Ni atom. The closed dots correspond to alloy targets and the open dots to composite targets.

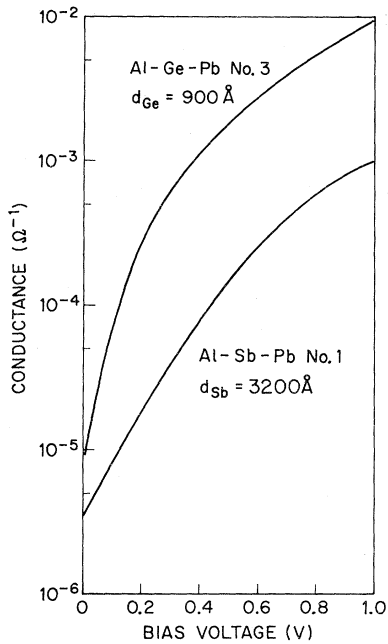


FIG. 8. Tunneling conductance as a function of bias voltage at 77°K for an Al-Ge-Pb and an Al-Sb-Pb junction, both deposited at 77°K (Al-Ge-Pb, etc., is a shorthand for Al-Al<sub>2</sub>O<sub>3</sub>-Ge-Pb).

only show the positive-bias side of the curves (meaning the *a*-semiconductor positive with respect to Al). The voltage drop across the *a*-semiconductor (known for MSM sandwiches, where *M* is Pb and *S* is *a*-Sb or *a*-Ge) was less than 5% of the total bias. Above 0.4 eV, where one is tunneling into extended states,<sup>11</sup> the voltage dependence of both curves in Fig. 8 is approximately the same. Below 0.4 eV the two curves are coming together, which can be stated more precisely by saying that the ratio of the conductance at 1 V to that at zero bias is about 10<sup>3</sup> for *a*-Ge and 300 for *a*-Sb. This is quite consistent with the fact that below 0.4 eV, where one is tunneling into localized states,<sup>11</sup> *a*-Sb has about<sup>1</sup> five times more localized states than *a*-Ge.<sup>4</sup> As the tunneling curve for *a*-Ge shown in Fig. 8 was analyzed as being consistent with a pseudogap of 0.8 eV,<sup>11</sup> one may conclude from the similarity of the tunnel curves of Fig. 8 that *a*-Sb has a pseudogap of the same magnitude.<sup>23</sup>

The fact stated above that one is tunneling into localized states at low bias voltages (<0.4 eV) is clearly demonstrated in Fig. 9 by the temperature dependence of the zero bias resistance. Indeed, the temperature dependence of the zero bias resistance follows Eq. (1) with a value of  $T_0$  ( $\approx 5 \times 10^6$ °K) only four times smaller than the value of  $T_0$  obtained from conductivity experiments.<sup>1</sup> This in

turn means that the tunneling density of localized states of *a*-Sb films deposited at 77°K is about four times higher than the density of states obtained from conductivity experiments. Worse discrepancies (factors of 20) were reported<sup>11</sup> for *a*-Ge, *a*-Si, and *a*-InSb films deposited at 77°K. These discrepancies were tentatively ascribed to the fact that tunneling probes the very first deposited layers, which are the most distorted and therefore contain a greater number of localized states. This explanation is supported by the fact that the value of  $T_0$  ( $1.9 \times 10^7$ °K) for an annealed *a*-Sb junction (Fig. 9) is in perfect agreement with the value of  $T_0$  obtained from conductivity experiments.<sup>1</sup> Agreement between tunneling and conductivity density of states has already been reported for an *a*-Si junction where the *a*-Si was deposited at room temperature.<sup>11</sup>

#### IV. SUMMARY

Using resistivity, tunneling, and doping experiments, we have shown that *a*-Sb is an amorphous semiconductor quite similar to *a*-Ge. This similarity has two important consequences. First, while theoretically *a*-Ge has been treated as a per-

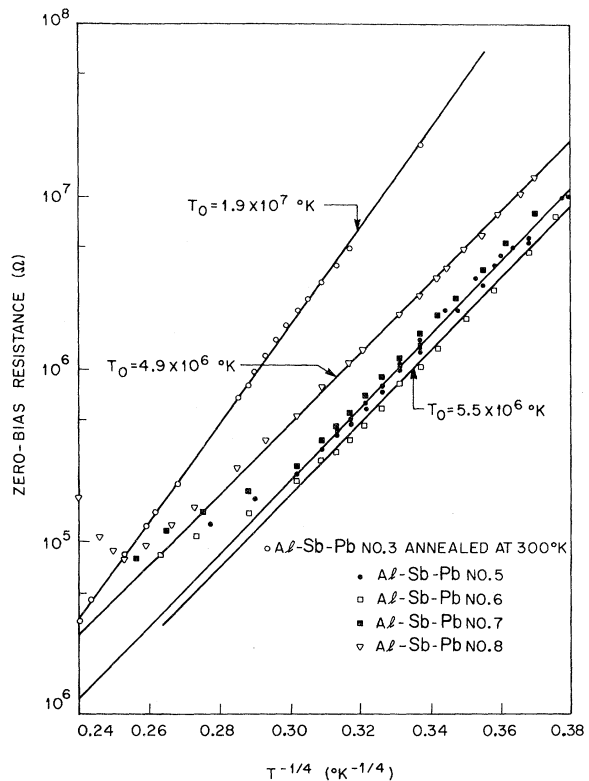


FIG. 9. Temperature dependence of the zero-bias conductance for various *a*-Sb junctions all deposited at 77°K; one junction (Al-Sb-Pb No. 3) was annealed at 300°K.

turbation of crystalline Ge, such an approach will not be possible for  $\alpha$ -Sb because crystalline Sb is a semimetal. Second, as  $\alpha$ -Sb is threefold coordinated, one may conclude that the thermally activated hopping conductivity is not limited to tetrahedrally bonded semiconductors. Consequently, this hopping conductivity could be found in a variety of other

structures and even in elements which are not semiconducting in the crystalline phase.

#### ACKNOWLEDGMENT

I would like to thank C. M. Antosh for his able technical assistance in obtaining the data.

<sup>1</sup>J. J. Hauser, Phys. Rev. B 9, 2623 (1974).

<sup>2</sup>N. F. Mott, Philos. Mag. 19, 835 (1969).

<sup>3</sup>P. A. Walley and K. Jonscher, Thin Solid Films 1, 367 (1968).

<sup>4</sup>J. J. Hauser and A. Staudinger, Phys. Rev. B 8, 607 (1973).

<sup>5</sup>M. Morgan and P. A. Walley, Philos. Mag. 23, 661 (1971).

<sup>6</sup>H. Richter, H. Berckhamer, and G. Breiteing, Z. Naturforsch. 9a, 236 (1956).

<sup>7</sup>Von H. Krebs and R. Steffen, Zeit. Anorg. Allg. Chemie 327, 224 (1964).

<sup>8</sup>N. F. Mott and E. A. Davis, *Electronic Processes in Non-Crystalline Material* (Clarendon, Oxford, England, 1971), p. 288.

<sup>9</sup>D. Shoenberg, Philos. Trans. R. Soc. Lond. A 245, 1 (1952).

<sup>10</sup>J. J. Hauser, Solid State Commun. 13, 1451 (1973).

<sup>11</sup>J. J. Hauser, Phys. Rev. B 9, 2544 (1974).

<sup>12</sup>I am indebted to J. E. Bernardini for the preparation of several alloy targets.

<sup>13</sup>J. J. Hauser, H. C. Theuerer, and N. R. Werthamer, Phys. Rev. 142, 118 (1966).

<sup>14</sup>The strongest line in a recrystallized Sb film is not the (102) or the (014) line, as for the random powders, but the (110) line because of the preferred orientation of the film.

<sup>15</sup>R. Ferrier and D. J. Herrell, J. Non-Cryst. Sol. 2, 278 (1970).

<sup>16</sup>W. Buckel and R. Hilsch, Zeit. Phys. 138, 109 (1954).

<sup>17</sup>B. Abeles, R. W. Cohen, and G. W. Cullen, Phys. Rev. Lett. 17, 632 (1966).

<sup>18</sup>J. J. Hauser, Phys. Rev. B 8, 2678 (1973).

<sup>19</sup>N. Barth, Zeit. Phys. 142, 58 (1955).

<sup>20</sup>We were not able to investigate these impurities because of the contaminating effects on the vacuum system of such impurities as Se and Te.

<sup>21</sup>One cannot specify in the present case the type of impurity level in the crystalline state, since crystalline Sb is a semimetal and not a semiconductor.

<sup>22</sup>V. Ambegaokar, B. I. Halperin, and J. S. Langer, Phys. B 4, 2612 (1972).

<sup>23</sup>The validity of this interpretation is further demonstrated by infrared-absorption measurements [S. H. Wemple, D. E. Aspnes, and J. J. Hauser (unpublished)] which yielded an optical gap of 0.7 eV.